Impulse force-measurement system

Y. Wang[1] · Z. Jiang[1]

Abstract
Shock tunnels are important ground test facilities that can generate high-enthalpy flow. Flight velocity at a high Mach number can be simulated for aerodynamic testing of chemically reacting flows. However, the application of these tunnels is limited due to the only milliseconds-long test duration, especially for aerodynamic force measurement using traditional strain gauge balances. This study presents an impulse force-measurement system, which was used for a large-scale test model to measure its drag in a high-enthalpy shock tunnel with an approximately 3–7-ms test time. Force tests were conducted for a cone in the JF-10 high-enthalpy shock tunnel in the Institute of Mechanics, Chinese Academy of Sciences. An integrated design of the impulse force-measurement system was proposed for load measurement over a short duration, for which a recommended design criterion is that the measurement period be a minimum of twice the period corresponding to the lowest natural frequency of the measurement system. The current measurement technique breaks the limitations of the application of the conventional strain gauge balance. As an integrated measuring system, the impulse force-measurement system expands the structural design concept of strain gauge balances. The impulse force-measurement system performed well in the present tests. The test results show differences from the numerical simulations and some data obtained in a conventional wind tunnel. A preliminary analysis was performed on the real gas effects on the aerodynamic force.

Keywords Shock tunnel · High enthalpy · Aerodynamic force measurement · Strain gauge balance

1 Introduction

In hypersonic aircraft design, the ground test is very important in providing aerodynamic data support. As an impulse facility, a shock tunnel can create very high-speed flow at very high temperature and pressure. Compared with the conventional hypersonic wind tunnel, the high-enthalpy hypersonic flow simulated in a shock tunnel is closer to real flight conditions. However, in force tests in the shock tunnel, because of the instantaneous flowfield and the short test time [1–4] (generally 500 µs–20 ms), mechanical vibration of the model–balance–support occurs and cannot be damped over the short duration. The inertial forces lead to low-frequency vibrations of the model, and its motion cannot be addressed by digital filtering. This implies restrictions on the model's

✉ Y. Wang
wangyunpeng@imech.ac.cn

1 State Key Laboratory of High Temperature Gas Dynamics
   (LHD), Institute of Mechanics, Chinese Academy of Sciences
   (CAS), Beijing 100190, China

size and mass because its natural frequencies are inversely proportional to its length scale. Regarding the measurement system, the lowest frequency of 1 kHz is required for the test time of typically 5 ms to obtain better measurement data [2]. The higher the natural frequencies, the better the justification for the neglected acceleration compensation. However, these conditions are very harsh for designing a high-stiffness structure of the model–balance–sting (MBS), particularly a measuring element for the axial load.

Based on these issues, many balance researchers proposed several special balances to measure aerodynamic forces, especially the axial force, in the impulse facilities with high enthalpy, that is, accelerometer balance [5–7], stress wave force balance [8–10], the free-flight measurement technique [11–16], and compensated balance [17]. However, owing to the very short test time, the mature technology was undeveloped for the force measurement in the shock tunnel with a short test duration. Based on the strain gauge sensor's higher accuracy and sensitivity, Wang et al. [18,19] designed a high-stiffness pulse-type balance using the strain gauge sensor and successfully carried out a series of force tests in a large-scale shock tunnel, which had a long test duration of more than 100 ms [20].

In this study, the impulse force-measurement system (iFMS) is built to obtain high-frequency balance signals. The structural characteristics of the iFMS and its integrated design were proposed to obtain a more optimized system for transient load measurement. An impulse strain gauge balance (iSGB), which is a part of iFMS and with a high-stiffness structure at the axial force element, was designed and used as a drag transducer in the short-duration impulse facility JF-10 [21,22]. Force tests were conducted for a large-scale cone with a 10° semivertex angle and a length of 375 mm in the JF-10 shock tunnel. The finite element method (FEM) was used for the analysis of the vibrational characteristics of the MBS structure, particularly for the axial element structure. The iFMS used in the test shows good performance, wherein the frequency of the MBS structure increases because of its stiff construction. The test results were analyzed to determine the effect of high-temperature gas through a comparison with the data obtained in nearly ten wind tunnels.

2 JF-10 high-enthalpy hypersonic shock tunnel

A shock tunnel is a type of impulsive ground facility, which uses a moving shock to generate high-temperature and pressure test gases. The stronger the moving shock is, the higher the test-gas enthalpy. Therefore, the benefits of a shock tunnel are that flight velocities up to Mach number 25 can be simulated [23]. To develop hypersonic vehicles, developing hypervelocity test facilities for ground experimental research is important. After more than 60 years of development, high-enthalpy facilities suitable for studying aerothermochemistry are still based on shock tunnels. For several decades, three types of high-enthalpy tunnels have been developed throughout the world. The first type is the heated-light-gas driven shock tunnel [24,25], the second type is the free-piston-driven high-enthalpy shock tunnel [26–28], and the third type is the detonation-driven high-enthalpy shock tunnel [29,30]. These hypersonic test facilities have been developed throughout the world, and such research facilities have provided valuable experimental data for years. The JF-10 shock tunnel at the Institute of Mechanics is the first high-enthalpy shock tunnel with a hydrogen and oxygen detonation-driven mode [21,31]. The JF-10 shock tunnel consists of three main parts. The first part is a driver with a length of approximately 6.225 m and a diameter of approximately 150 mm. The second part is a driven section of 12.5 m in length and 100 mm in diameter, and the last part is a conical nozzle with a 500-mm-diameter exit. This facility can simulate some complicated physical and chemical phenomena in hypersonic flight at high altitudes and features a high-enthalpy test flow, a total enthalpy range of 15–25 MJ/kg, a total temperature range of 7500–9500 K, a total pressure range of 10–80 MPa, and an effective test time range of 3–7 ms.
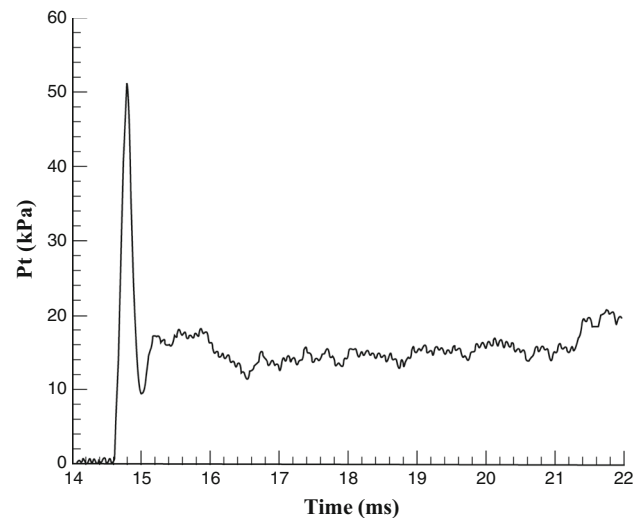
**(a)** Pitot pressure history measured versus time
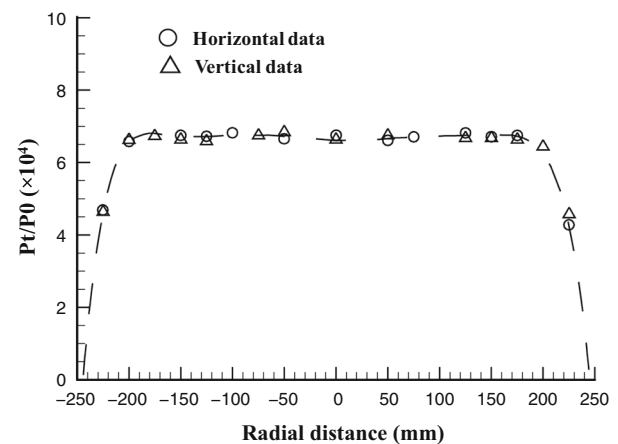
(b) Radial pressure distributions

Fig. 1 Pitot pressure measurements at the cross section of the nozzle exit in the JF-10 nozzle flow (Pt and P_0 are Pitot pressure and total pressure, respectively)

Figure 1 shows the Pitot pressure history and its distributions at the cross section of the nozzle exit obtained by calibration tests of the flowfield. Given the Pitot pressure results, the stagnation temperature of 7561 K is used in the present tests and in simulations performed with the computational fluid dynamics (CFD) technique. Hypersonic flows in the nozzle central area appear quite uniform if evaluated from the viewpoint of a Pitot pressure distribution. This uniform flow area is found to be approximately 700 mm in length and 400 mm in diameter [31].

3 Integrated design of the iFMS and experimental description

To obtain the multi-cycle signal, the stiffness of the measurement system should be increased. The MBS structure
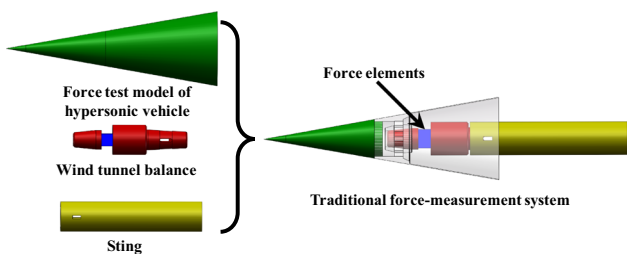
(a) The structure of traditional force-measurement system
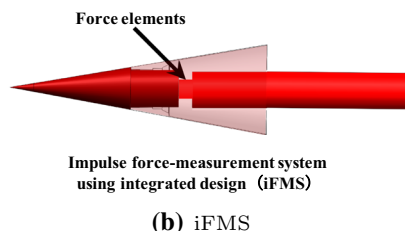
(b) iFMS

Fig. 2 Structures of the traditional force-measurement system and the present integrated design

Fig. 3 Diagrams of the iFMS and iSGB used in drag tests

needs to be optimized using the FEM technique. Therefore, we built an iFMS that includes the test model with a high-stiffness and pulse-type balance (i.e., iSGB) with a high-strength sting. The traditional wind tunnel balance is used as a part of the measuring system (i.e., MBS). However, the current force balance, namely the iFMS, belongs to the concept of a complex measuring system as a whole. Figure 2 shows the structural difference between the traditional force-measurement system and the present iFMS. The iFMS using the same color (red color) is a whole structure with integrated design. The traditional force-measurement system is a separate assembly structure, where the model, balance, and sting are designed separately. The traditional force-measurement system is marked with different colors for the different parts in Fig. 2.

In the iFMS design, determining the structures of the test model and sting is relatively easy. The iSGB design is the most complicated, particularly for the measuring element of the axial force. In comparison with the piezo-electric sensor, the strain gauge has a sufficient frequency response and higher accuracy and sensitivity. We attempted to use a strain gauge transducer to measure the aerodynamic loads in the impulse ground facility for a test time of only a few milliseconds. In our present study, the foil strain gauge, which has enough high frequency response for the case of high-frequency characteristics, is used in the high-stiffness balance. Our previous experimental and computational results in the long-test-duration shock tunnel JF-12 (with more than a 100-ms test duration) [18,19] show that the iSGB, with the optimized structures, can be used to obtain satisfactory results in the shock tunnel. Therefore, an iSGB, which is used in JF-12, was developed and redesigned for
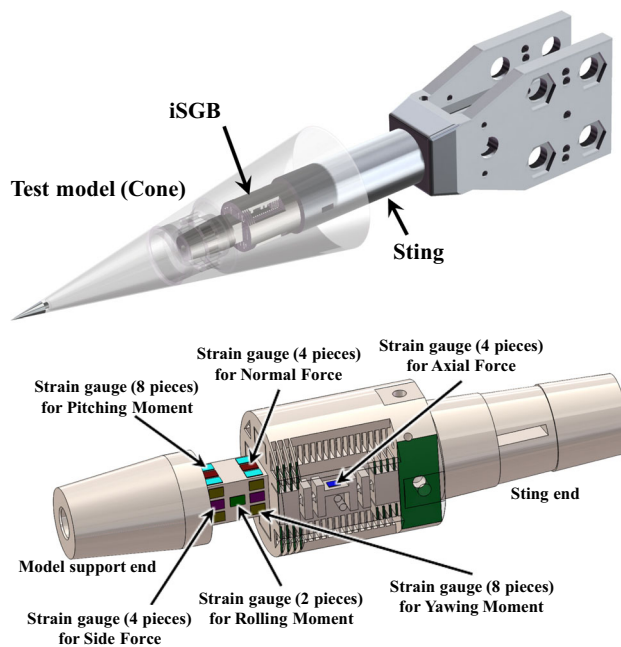
the drag measurements in a short-duration shock tunnel. The iSGB was optimized from the aspect of the measuring element of the axial load, and its performance is excellent given a Π-shaped beam with high sensitivity. (See the axial force element in Fig. 3.) From the FEM simulations, iSGB has a very high frequency at the axial element (more than a 2000 Hz modal frequency) because of the hundreds of support pieces in the main balance body.

Figure 3 shows the details of the iFMS and its measuring element, that is an iSGB. The iSGB is a three-component (i.e., normal force, axial force, and pitching moment) sting balance with a diameter of 53 mm. Only one rectangular beam is used to measure the two components, except for the axial force. This structure is the simplest, can increase the balance stiffness, and can simplify the vibration mode.

In the shock tunnel, the structural vibration of the measuring system is caused by starting up the nozzle flow. This process is very complex and usually takes almost 1 ms. However, in the following 3–7 ms, the flow will become pseudo-steady. Therefore, the next difficult task is to design the high-stiffness sting to support the balance and test model. In the design of the iFMS, we proposed a design criterion:

$$f_i = \frac{2}{t^*}, \tag{1}$$

where f_i and t^* are the modal frequency of iFMS in the i-th component (e.g., axial load) and the test duration of the impulse facility, respectively. Therefore, in the case of JF-10 with an effective test time of 4 ms, the vibrational frequency of iFMS in the axial component should be more than 500 Hz

so that we can find at least two cycles in the balance output signal.

To carry out the force test in the impulse facility, the weight of the test model is a very important factor in determining whether good results can be obtained. The present cone model with the 10° semivertex angle is made of aluminum alloy. Its full length is 375 mm, and it has a maximum wall thickness of 1 mm. Therefore, its total mass is only 550 g. A lighter model will significantly increase the vibration frequency of the force-measurement system.

The starting characteristics of the shock tunnel are an important part of the integrated design in this study. Before the design of the iFMS, the starting process of the nozzle flow in the shock tunnel was also analyzed using CFD simulations because of the large impact loads acting on the test model. Therefore, the capacity of the axial force is 500 N given the impact characteristics of the starting process in the JF-10 shock tunnel.

Prior to the shock tunnel run, the three-dimensional design of the iFMS is modeled. A series of computations, including the static structure, dynamics, and modal analysis, is conducted using finite element analysis. The numerical results can be used to estimate the experimental results, such as the iFMS vibrational frequency and cycle number, within the short test time. Because of the optimized iFMS, the frequency f_i in the present study reaches more than 1050 Hz in the axial direction. Therefore, at least four cycles should be found in the balance signal within the short test time of $t^* = 4$ ms.

4 Numerical rebuilding of freestream measurement

Some freestream parameters are very difficult to measure directly, such as Mach number, density, static temperature, and so on. In conventional low-enthalpy hypersonic wind tunnels, the above parameters are also calculated through the isentropic relationship. However, in the high-enthalpy wind tunnel, these freestream parameters cannot be simply obtained through an isentropic relationship because of the large errors in the case with real gas effects. Therefore, in this study, we performed the more accurate chemical non-equilibrium CFD simulations in the flowfield of the overall nozzle and the test section, that is the numerical rebuilding of freestream measurements.

For high-enthalpy facilities and similar ones, Grabau et al. [32] suggested an alternative rebuilding method, involving the additional measurement of the stagnation point heat flux on a spherical geometry located in the test section. This method of numerical prediction has been applied to the VKI Longshot gun tunnel [33]. For nitrogen operation, real gas equations of state [34,35] have been used in order to accu-
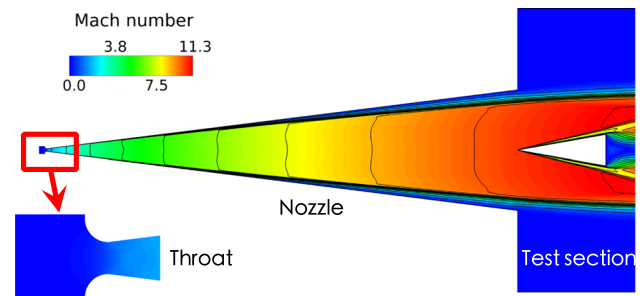

Fig. 4 Mach number distributions obtained by CFD simulation

rately describe the enthalpy and entropy of the dense gas prior to the nozzle expansion.

The effect of the non-equilibrium flow was considered in the calculation [36–39]. Two-dimensional axisymmetric compressible conservation equations were employed to calculate the chemical non-equilibrium flows. The Spalart–Allmaras [40] turbulence model was employed to evaluate the effects of the turbulent boundary layer. For the simulations of chemical non-equilibrium effects in high-temperature air, seven species (N_2, O_2, N, O, NO, NO^+, and e^-) are employed in the thermochemical non-equilibrium model. The stagnation conditions, such as the stagnation pressure and temperature, were the same as those in the present tests in the JF-10 shock tunnel.

Figure 4 shows the Mach number distributions by the numerical rebuilding method, which includes a cone with an angle of attack 0°.

In the numerical prediction, the rear base pressure of the cone is compared between the perfect gas and real gas. The case of real gas is a little higher than the perfect gas case (see Fig. 5). Compared with the pressure distribution on the cone surface (along x-direction), the cone base pressure is reduced by about one order of magnitude. Therefore, the base pressure of the cone has a little influence on the overall drag result.

5 Drag measurement and data analysis

Because the cone model has a large volume of test data and theoretical analysis results, it is often used as a standard model for the flowfield calibration of new or modified wind tunnels. In the drag tests, the average stagnation pressure is 13.6 MPa, the average stagnation temperature is 7600 K, and the corresponding total enthalpy is 16.7 MJ/kg. These conditions result in an average freestream Mach number of 11. The drag measurements for the cone were conducted at an angle of attack nearly of 0°, with an approximately 0° sideslip angle. By the evaluation, the uncertainty of angle of attack is approximately ±0.01°, while the case of sideslip angle is less than ±0.05°, which can be controlled through
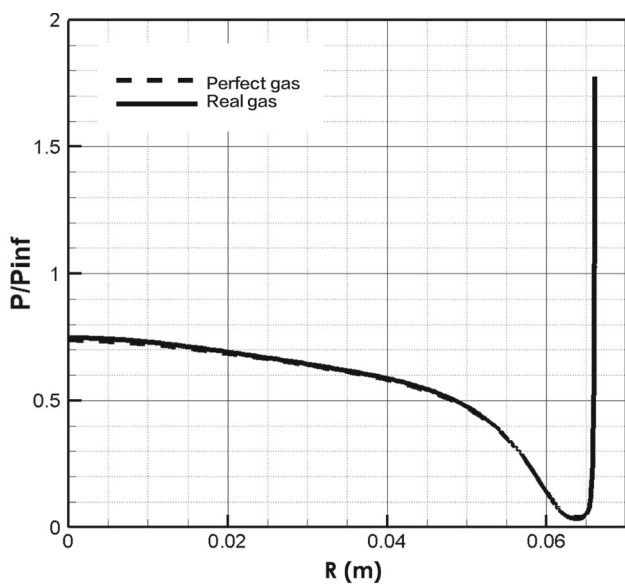
(a) Base pressure of the cone
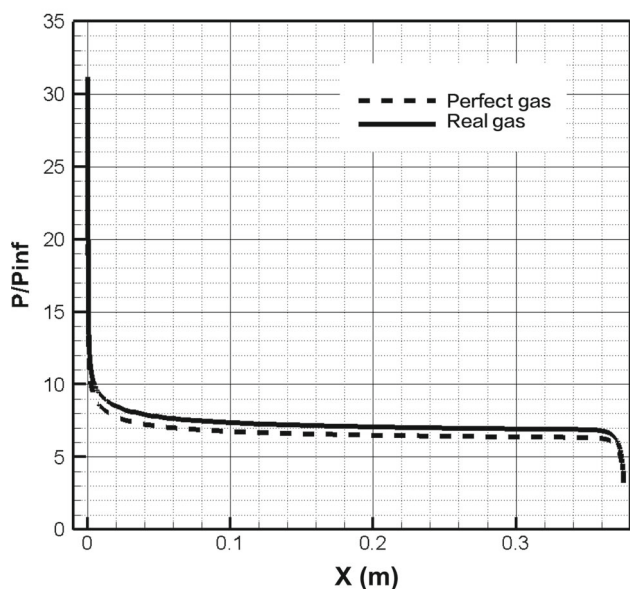
(b) Pressure distribution on the cone surface

Fig. 5 Pressure distributions between the cases of perfect gas and real gas (here, P_{inf} and R are the uniform flow pressure and the cone's bottom radius, respectively)

a mechanical assembly. In the current tests, the actual measured value of the angle of attack is maximum 0.011° and the sideslip angle is not greater than 0.05°.

Figure 6 shows a photograph of the 375-mm cone model mounted in the test section.

Before the drag tests in the JF-10 high-enthalpy shock tunnel, we carried out a hammer test to check the modal frequency. A force hammer with a piezoelectric sensor was employed, and the test focused on the axial structure (i.e., along the drag direction). In the test, the acceleration sensor
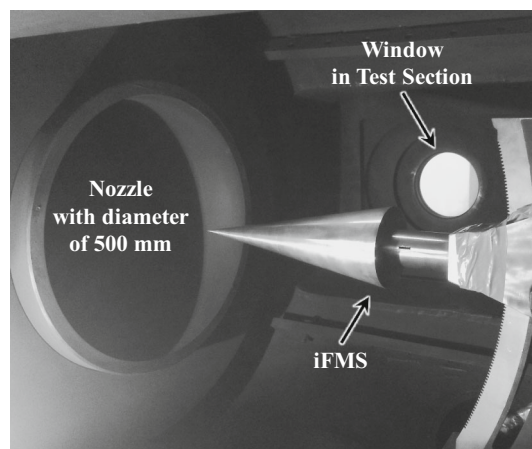

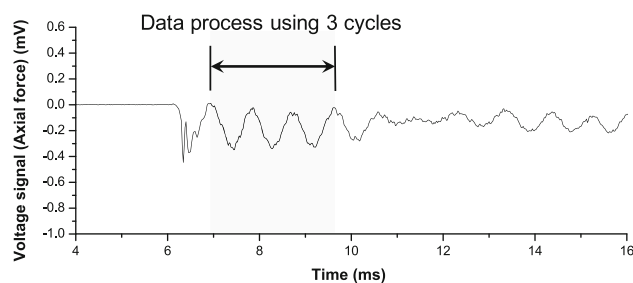**Fig. 6** Photograph of the iFMS in JF-10's test section

Fig. 7 Voltage signal of the iSGB and its processing by WSF method

was arranged in the axial direction. The vibrational frequency from the results of the hammer test is 1095 Hz, which is consistent with the frequency of the previous analysis using the FEM simulation.

In our study, a method for the test data processing, namely *wave system fitting* (WSF) [41], is used and two to three cycles in the balance output signal are enough for the data processing.

Based on this method of data processing, the effect of inertial vibration with the low frequency can be decreased. Also, the integer number of cycles can be found during the test time so that the averaged processing of balance signals is reasonable and reduces the processing error.

Figure 7 shows the balance voltage signal from a force test in the shock tunnel. As the figure indicates, four complete cycles exist within the effective test time of 4 ms. The frequencies of the balance signal were found from the test findings using fast Fourier transformation analysis, and the averaged value is 1108 Hz. Obviously, this result is consistent with the results of the FEM analysis (1050 Hz) and the hammer test (1095 Hz).

Furthermore, good repeatability is observed during the shock tunnel testing, in which the standard deviation σ_{C_D} of the drag coefficient is 0.0042, which is less than 4.0%. Here, the following equation is used to calculate the standard deviation σ_{C_D}:
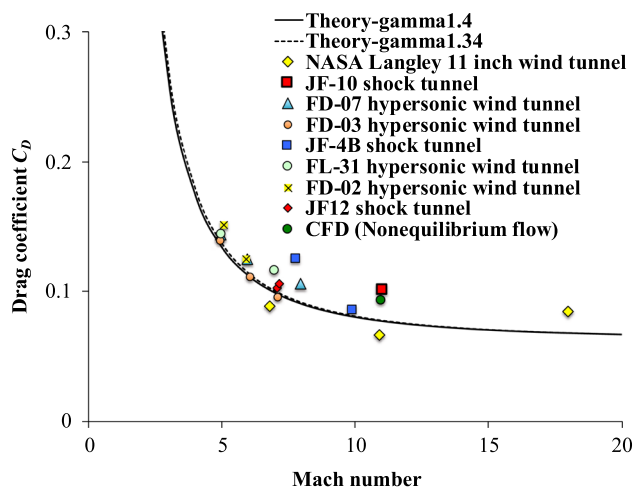
Fig. 8 Comparison of the drag test results (the axial force at the 0° angle of attack)

$$\sigma_{C_D} = \sqrt{\sum_{i=1}^{n} \frac{(C_{Di} - \bar{C}_D)^2}{n-1}} \qquad (2)$$

where $\bar{C}_D$ is the averaged value of drag coefficients of n tests; in the present study, $n = 8$. Therefore, the iFMS also shows good performance in terms of test precision.

The C_D is calculated by the following equation:

$$C_D = \frac{D}{qS} \qquad (3)$$

where D is the drag (axial force) and q and S represent the dynamic pressure and the reference area of the model, respectively.

Figure 8 shows the present drag result compared with some data from the conventional hypersonic wind tunnels [42–44], impulse facilities [18,19], theoretical analyses, and CFD simulation. In the theoretical estimates, Cheng's cone theory [45,46] is employed to predict changes due to variations in the ratio of specific heats γ. The present analyses show little effect on the ratio of specific heats γ, where the drag in the case of $\gamma = 1.34$ appears to be a little different than that in the $\gamma = 1.4$ case. Both curves are practically the same and can hardly be distinguished from one another. In the theoretical analysis, the effect of high temperature on hypersonic flow will cause the change of γ. Here, $\gamma = 1.34$ corresponds to the equilibrium flow state with the total temperature of 7600 K, while $\gamma = 1.4$ is the specific heat ratio of the perfect gas. The calculated result of the drag is also shown in Fig. 8. The measured drag force was 9.5% higher than the value from CFD and 31% higher than the theoretical value.

The test results inherit some uncertainties due to the systematic and random errors in determining the freestream properties, performing the force measurement, calibrating

the balance, etc. In this paper, a preliminary analysis of the uncertainty of the test results was also performed. Each type of error limit is combined with each type of error limit of the measured variables and constants, principally because they are independent parameters. In this study, the drag coefficient is a function of the measured values of dynamic pressure and balance axial force. In this study, a ball free-flight method is employed to directly measure the dynamic pressure through the image processing technique, in which the ball's movements (i.e., free-flight) in the flowfield are recorded using synchronized high-speed photography [47]. The dynamic pressure q measured using this method can ensure the successful avoidance of the introduction of parameter errors in the hypersonic flowfield, such as errors confirmed by measuring the total pressure, total temperature, Pitot pressure, and wall pressure in the test section. In this study, the dynamic pressure uncertainty (95% CI) is ± 0.533 kPa, which is approximately 5% of the averaged q. Therefore, the uncertainty assessment of testing drag becomes simple and more accurate.

The relative uncertainty in C_D, denoted U_{C_D}, is written as

$$U_{C_D} = \pm\sqrt{P_{C_D}{}^2 + B_{C_D}{}^2} \qquad (4)$$

where P_{C_D} and B_{C_D} are the precision limit and bias limit of C_D, respectively [48–50]. The present results were analyzed using the 90% confidence interval (CI). The confidence interval is designated prior to examining the data. Most commonly, the 95% CI is used. Other CI also can be used; for example, 99% CI is used for evaluating precision in the force tests in the high- and low-speed traditional wind tunnels, because the test duration is long enough in the traditional wind tunnel and the force-measurement technique is very mature in low-speed wind tunnels. However, for the high-enthalpy impulse facilities, the test time is very short (normally several milliseconds) in the shock tunnel due to the impulse characteristics. The technique of force measurement is also not mature in the impulse facilities. Therefore, 90% confidence range is employed in this study.

Through post-processing, a conservative assessment result is $U_{C_D} \leq \pm 0.0089$, that is $U_{C_D} \leq \pm 8.5\%$ C_D (90% confidence interval). It demonstrates the reliability of the drag measurement in the JF-10 high-enthalpy hypersonic shock tunnel.

6 Discussions on aerodynamic force with high-temperature effects

6.1 General thought on drag

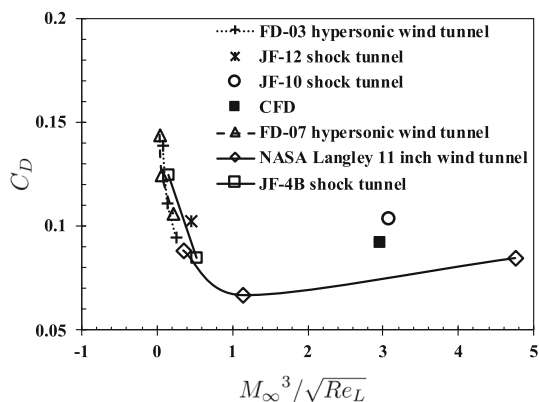It is well known that, for the drag results, one part is attributable to pressure distributions over the body surface

Fig. 9 Viscous interaction of the drag coefficient on the cones

Table 1 Cones' length and flow conditions in different wind tunnels

Wind tunnels	L (m)	M_∞	Re (L)	T_0 (K)
FD-03 hypersonic wind tunnel [19,44]	0.141	4.94	3.31×10^6	350
		6.07	2.66×10^6	465
		7.10	2.15×10^6	596
FD-07 hypersonic wind tunnel [19,44]	0.340	4.96	14.3×10^6	375
		5.95	12.3×10^6	490
		7.96	6.13×10^6	756
JF-12 shock tunnel [18,19]	0.75	7.07	0.60×10^6	2200
JF-10 shock tunnel	0.375	11.00	0.19×10^6	7600
NASA Langley 11-inch wind tunnel [42,43]	0.216	6.80	0.81×10^6	630
		10.90	1.31×10^6	–
		18.00	1.51×10^6	–
JF-4B shock tunnel [53]	0.284	7.80	9.94×10^6	895
		9.90	3.41×10^6	–

and another part is attributable to skin friction, which is a result of viscosity. Anderson [51] makes a conclusion that the pressure distributions are always somewhat insensitive to chemically reacting effects, while the chemical reactions have the strongest effect on temperature. The kinetic energy of a high-speed, hypersonic flow is dissipated by the influence of friction within a boundary layer. The extreme viscous dissipation that occurs within a hypersonic boundary layer can create high temperatures, which can excite vibrational energy internally within molecules and cause dissociation and even ionization within the test gas if the temperature increases continuously [51]. Therefore, the viscosity is analyzed in detail in the current paper as the main effective factor.

Compared to the blunt body (like a reentry vehicle), the larger percentage of the cone's drag is attributable to the result of viscosity. Therefore, the viscous interaction is analyzed using a parameter $M_\infty^3/\sqrt{Re_L}$, which can be used for the evaluation of the viscous interaction on the aerodynamic characteristics. If the value of $M_\infty^3/\sqrt{Re_L}$ is low, the actual pressure distribution is mainly governed by inviscid flow effects. In contrast, a high value indicates that viscous interactions should be important [52].

Figure 9 shows the difference of the cones' drag due to the viscous interaction. Some details of the freestream conditions in the low- and high-enthalpy wind tunnels are shown in Table 1.

Based on the above analysis, the present drag obtained from JF-10 shows the importance of viscous interaction. Compared with data by Langley 11-inch hypersonic wind tunnel (the case of Mach number 10.9, which is almost same with JF-10's conditions), the present result by the JF-10 shows more strong effects of the viscous interaction. Koppenwallner [54] shows that the viscous interaction effects on the skin friction and heat transfer coefficients are correlated by a parameter $M_\infty/\sqrt{Re_L}$. It means that both skin friction and heat transfer are increased by viscous interaction. Anderson [51] shows that the pressure is strongly dependent on the

mechanical aspects of the flow and essentially uninfluenced by chemically reacting effects. It means that the pressure distributions are always somewhat insensitive to the chemically reacting effects. CFD results shown in Fig. 5 also confirm this point. In contrast, the ratio of the cone surface density to freestream density is greatly affected by the chemical reactions. The effect of chemical reactions increases the density ratio compared to the $\gamma = 1.4$ case, which implies that the shock layer thickness will be smaller for the chemically reacting case. This makes it obvious that the velocity gradient becomes larger due to the thinner boundary layer, which also leads to an increased shear force.

Based on the total temperature conditions shown in Table 1, the larger drag of cone in the JF-10 (see Figs. 8 and 9), with the hypersonic and high-enthalpy condition, may be caused by the high-temperature effects, that is the effects of chemical reactions, as the preliminary judgment in the present study. By checking the CFD results, the static temperature of uniform flow is 400 K, and the temperature in the thin hypersonic boundary layer is approximately 7000 K in JF-10. Therefore, as previously discussed, the vibrational energy is excited and the oxygen is dissociated within a chemically reactive boundary layer.

Figure 10 shows the high-temperature test gas over the cone, and the bright light is generated on the cone's surface because of the high-enthalpy condition. Because oxygen begins to dissociate above 2000 K, it is virtually completely dissociated above 4000 K [51]. Because of the high temperature in the hypersonic boundary layer, the viscosity increases
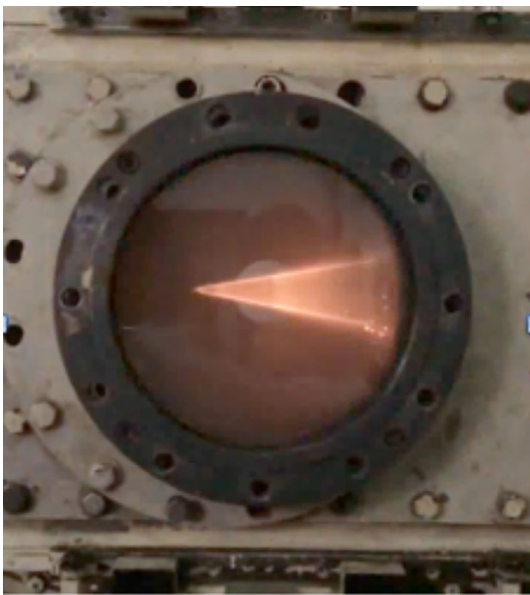
Fig. 10 Test flow over the cone during a shock tunnel run

and the shear force (skin friction) on the model surface becomes large, which results in a larger drag.

6.2 Drag measurements in JF-12

In this section, a large cone test at relatively low total temperature condition and a blunt body model are analyzed to compare the drag test of the cone under high-enthalpy conditions in JF-10.

In Figs. 8 and 9, the data from the JF-12 were obtained at Mach number 7 by using the iSGB and a larger cone; the length is 750 mm. It is employed in the JF-12 long-test-duration shock tunnel with a total temperature of 2200 K. From the data comparison, the viscous interaction is relatively small in the cone test of the JF-12. In addition, in order to examine the accuracy of the present iFMS, a standard model in the force test, HB-2 [55], was employed for measuring the drag using the current iFMS in the JF-12 shock tunnel, which has a blunt forebody. At the same time, the drag data of HB-2 test also can be used to further analyze the viscous interaction.

Figure 11 shows the HB-2 test model for the drag test using the present iFMS in the JF-12 shock tunnel. HB-2 is a standard hypersonic ballistic correlation model, which has been examined to establish reference characteristics for use in the correlation of experimental results among the various aerodynamic facilities. This ballistic correlation model was first voiced at the joint meeting of AGARD (The Advisory Group for Aeronautical Research and Development) and STAI (Supersonic Tunnel Association International) held in France during September 1959 [55]. The current model used
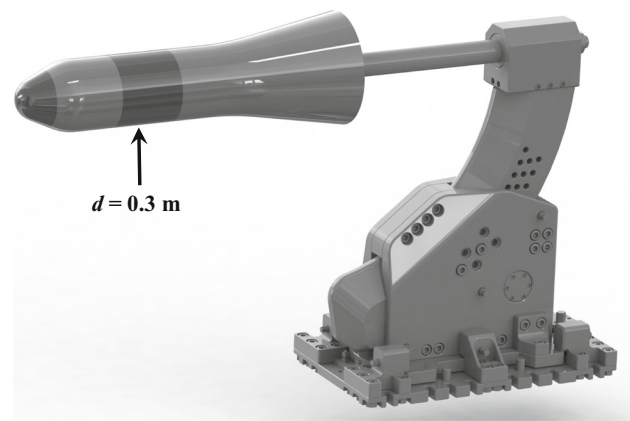

Fig. 11 Standard force model HB-2

Table 2 Comparison of the drag data in the VKF (the von Karman gas dynamics facility) 12 in. $\times$ 12 in. hypersonic tunnel E and the JF-12 hypersonic shock tunnel

Wind tunnels	d (m)	M_∞	Re (d)	T_0 (K)	C_D
VKF [55]	0.0635	7.07	6.0×10^5	–	0.5320
JF-12	0.3	6.98	0.9×10^5	3430	0.5398

in this study has a forebody diameter d of 0.3 m and a length of 4.9 times the diameter d.

In the force test of the model HB-2, the standard deviation of the drag coefficient is approximately 1.0%, and $U_{C_D} \leq \pm 5.0\%$ C_D (95% confidence interval) due to the long test duration of the JF-12 shock tunnel, which is greater than 100 milliseconds during a shock tunnel run. Therefore, the accuracy of the current force-measurement system, iFMS, has been further verified. Furthermore, compared with the data by VKF (tunnel E), the viscous parameter $M_\infty^3/\sqrt{\mathrm{Re}_L}$ is larger in the JF-12's test due to a higher total temperature, which is more than 3400 K (see Table 2). A higher-enthalpy condition leads to a lower Reynolds number in the JF-12 so that the viscous interaction becomes larger.

The hypersonic viscous interaction is analyzed in the works of Anderson [51] and Hirschel [56]. Anderson [51] shows that shear stress is a viscous flow phenomenon and the skin friction drag can be obtained by calculating the shear stress distribution over the surface of hypersonic aerodynamic shapes. In his work, a conclusion is that the viscous interactions can have important effects on the surface pressure distribution, and the skin friction and heat transfer are increased by viscous interaction. The pressure distributions are always somewhat insensitive to chemically reacting effects, as noted earlier, while the chemical reactions have the strongest effect on temperature. Therefore, in the current preliminary analysis, the reason for the higher drag is considered to be an increase in skin friction drag. Hirschel's work [56] also shows that the turbulent skin friction is lowest for the per-

fect gas, adiabatic wall case, and largest (approximately 45 percent larger) for the radiation cooling case, which means that the high-temperature real gas effects can play a non-negligible role regarding turbulent skin friction. During the shock tunnel test, the test flow has not reached equilibrium in the boundary layer and the temperature in there continues to increase because of the strong effect of the chemical reactions. At the same time, the skin friction also increases due to the high-temperature real gas effects. Obviously, this phenomenon becomes inconspicuous in the results of conventional hypersonic wind tunnel tests because of the very low total temperature.

7 Summary

In this study, the designed iFMS can obtain multiple cycles of the balance signal and can measure more accurate results to enable a further understanding of the complex phenomenon in a hypersonic flows with higher enthalpy. The test results highlight the effects of the high-enthalpy flow on aerodynamic drag. The results indicate that the high-temperature effects should not be ignored when the total enthalpy (or the total temperature) is high in the hypersonic (or hypervelocity) flow.

An impulse force-measurement system was designed and optimized via FEM analysis. The aerodynamic drag of a large-scale cone was measured using this iFMS in the high-enthalpy hypersonic shock tunnel JF-10 with an approximately 4-ms test time. The strain gauge balances are broadly used for force measurement in the conventional wind tunnel as a mature technology; however, they seldom work in the shock tunnel or other impulse facilities. The drag balance is very difficult to design and use in a short-duration ground facility given the low-frequency vibrations of the MBS by the inertial force. In the present study, the high-stiffness iSGB used in the test shows good performance, wherein the frequency of the iFMS increases because of its stiff construction. Force tests were conducted for a cone with a $10°$ semivertex angle and a length of 375 mm. An FEM simulation and the hammer test were employed for the analysis of the vibrational characteristics of the iFMS to examine a sufficient number of cycles (the axial vibration frequency) during a short-duration test for the axial force signal. The design criterion for the balance's structure with a higher frequency is proposed to ensure at least two cycles in the balance signal during the effective test time. The structural performance of the present iSGB is in full compliance with the requirements of drag measurement during 4 ms. Therefore, the iFMS with an optimized structure breaks the limitations of the applications of the conventional strain gauge balance and can be used for the large-scale model in the force tests in the short-duration hypersonic shock tunnel.

The test results were analyzed to determine the effect of high-temperature gas through a comparison with the data obtained in nearly ten wind tunnels. The standard deviation of the drag coefficient is small, which is less than 4.0%, and 90% CI $U_{C_D} \leq \pm 8.5\% \, C_D$. In addition, in a long-test-duration shock tunnel JF-12, the drag of the standard model HB-2 was measured for further verification of the iFMS's performance. In the force tests of the model HB-2, the standard deviation of the drag coefficient is approximately 1.0%, and 95% CI $U_{C_D} \leq \pm 5.0\% \, C_D$.

The present drag obtained by the JF-10 force test shows more strong effects of the viscous interaction. The preliminary analysis of this study is that, due to the real gas effects, the increase in skin friction drag may be one of the main reasons for the larger overall drag of the cone model. The detailed mechanism on the aerodynamic drag with real gas effects needs to be studied in more depth.

References

1. Arrington, P.J., Joiner, R.J., Henderson, A.J.: Longitudinal characteristics of several configurations at hypersonic mach numbers in conical and contoured nozzles. NASA TN D-2489 (1954)
2. Bernstein, L.: Force measurement in short-duration hypersonic facilities. AGARDograph No. 214 (1975)
3. Naumann, K., Ende, H., Mathieu, G., George, A.: Millisecond aerodynamic force measurement with side-jet model in the ISL shock tunnel. AIAA J. **31**, 1068–1074 (1993). https://doi.org/10.2514/3.11730
4. Naumann, K., Ende, H.: A novel technique for aerodynamic force measurement in shock tubes. International Congress on Instrumentation in Aerospace Simulation Facilities, Gottingen, West Germany, pp. 535–544 (1989). https://doi.org/10.1109/ICIASF.1989.77710
5. Joarder, R., Jagadeesh, G.: A new free floating accelerometer balance system for force measurements in shock tunnels. Shock Waves **13**, 409–412 (2003). https://doi.org/10.1007/s00193-003-0225-y
6. Saravanan, S., Jagadeesh, G., Reddy, K.P.J.: Aerodynamic force measurement using 3-component accelerometer force balance system in a hypersonic shock tunnel. Shock Waves **18**, 425–435 (2009). https://doi.org/10.1007/s00193-008-0172-8
7. Sahoo, N., Mahapatra, D.R., Jagadeesh, G., Gopalakrishnan, S., Reddy, K.P.J.: An accelerometer balance system for measurement of aerodynamic force coefficients over blunt bodies in a hypersonic shock tunnel. Meas. Sci. Technol. **14**, 260–272 (2003). https://doi.org/10.1088/0957-0233/14/3/303
8. Robinson, M.J., Schramm, J.M., Hannemann, K.: Design and implementation of an internal stress wave force balance in a shock tunnel. CEAS Space J. **1**, 45–57 (2011). https://doi.org/10.1007/s12567-010-0003-5
9. Sanderson, S.R., Simmons, J.M., Tuttle, S.L.: A drag measurement technique for free-piston shock tunnels. 29th Aerospace Sciences Meeting, Reno, NV, U.S.A., AIAA Paper 91-0549 (1991). https://doi.org/10.2514/6.1991-549

10. Mee, D.J., Daniel, W.J.T., Simmons, J.M.: Three-component force balance for flows of millisecond duration. AIAA J. **34**(3), 590–595 (1996). https://doi.org/10.2514/3.13108

11. Seiler, F., Mathieu, G., George, A., Srulijes, J., Havermann, M.: Development of a free flight force measuring technique (FFM) at the ISL shock tube laboratory. 25th International Symposium on Shock Wave, Bangalore, India (2005)

12. Wey, P., Bastide, M., Martinez, B., Srulijes, J., Gnemmi, P.: Determination of aerodynamic coefficients from shock tunnel free-flight trajectories. 28th Aerodynamic Measurement Technology, Ground Testing, and Flight Testing Conference, New Orleans, USA, AIAA Paper 2012-3321 (2012). https://doi.org/10.2514/6.2012-3321

13. Martinez, B., Bastide, M., Wey, P.: Free-flight measurement technique in shock tunnel. Proceedings of the 30th Aerodynamic Measurement Technology and Ground Testing Conference, Atlanta, USA, AIAA Paper 2014–2523 (2014). https://doi.org/10.2514/6.2014-2523

14. Tanno, H., Komuro, T., Sato, K., Fujita, K., Laurence, S.J.: Free-flight measurement technique in the free-piston shock tunnel hiest. Rev. Sci. Instrum. **85**, 045112 (2014). https://doi.org/10.1063/1.4870920

15. Tanno, H., Komuro, T., Sato, K., Itoh, K., Yamada, T.: Free-flight tests of reentry capsule models in free-piston shock tunnel. 43rd Fluid Dynamics Conference, San Diego, CA, AIAA Paper 2013-2979 (2013). https://doi.org/10.2514/6.2013-2979

16. Laurence, S.J., Karl, S.: An improved visualization-based force-measurement technique for short-duration hypersonic facilities. Exp. Fluids **48**, 949–965 (2010). https://doi.org/10.1007/s00348-009-0780-9

17. Marineau, E., MacLean, M., Mundy, E., Holden, M.: Force measurements in hypervelocity flows with an acceleration compensated strain gage balance. J. Spacecr. Rockets **49**(3), 474–482 (2012). https://doi.org/10.2514/1.A32041

18. Wang, Y.P., Liu, Y.F., Luo, C.T., Jiang, Z.L.: Force measurement using strain-gauge balance in a shock tunnel with long test duration. Rev. Sci. Instrum. **87**, 055108 (2016). https://doi.org/10.1063/1.4950781

19. Wang, Y.P., Liu, Y.F., Jiang, Z.L.: Design of a pulse-type strain gauge balance for a long-test-duration hypersonic shock tunnel. Shock Waves **26**(6), 835–844 (2016). https://doi.org/10.1007/s00193-015-0616-x

20. Jiang, Z., Yu, H.: Theories and technologies for duplicating hypersonic flight conditions for ground testing. Natl. Sci. Rev. **4**, 290–296 (2017). https://doi.org/10.1093/nsr/nwx007

21. Jiang, Z., Zhao, W., Wang, C., Takayama, K.: Forward-running detonation drivers for high-enthalpy shock tunnels. AIAA J. **40**, 2009–2016 (2002). https://doi.org/10.2514/2.1533

22. Jiang, Z., Chang, L., Zhang, F.: Dynamic characteristics of spherically converging detonation waves. Combust. Flame **16**, 253–267 (2007). https://doi.org/10.1007/s00193-006-0066-6

23. Stalker, R.: Modern developments in hypersonic wind tunnels. Aeronaut. J. **110**(1103), 21–39 (2006). https://doi.org/10.1017/S0001924000004346

24. Holden, M.: Design, development and calibration of the lens facility. AFOSR-TR 94–0161 (1994)

25. Holden, M.: Recent advances in hypersonic test facilities and experimental research. AIAA/DGLR 5th International Aerospace Planes and Hypersonics Technologies Conference, Munich, Germany, AIAA Paper 93-5005 (1993). https://doi.org/10.2514/6.1993-5005

26. Rose, P.H.: Development of the calorimeter heat transfer gauge for use in shock tubes. Rev. Sci. Instrum. **29**(7), 557–564 (1958). https://doi.org/10.1063/1.1716258

27. Stalker, R.: A study of the free-piston shock tunnel. AIAA J. **5**(12), 2160–2165 (1967). https://doi.org/10.2514/3.4402

28. Stalker, R.J.: Shock tunnel for real gas hypersonics. Aerodynamics of Hypersonic Lifting Vehicles, AGARD Conference Proceedings No. 428, Bangalore, India (1987)

29. Yu, H.R., Esser, B., Lenartz, M., Gronig, H.: Gaseous detonation driver for a shock tunnel. Shock Waves **2**, 245–254 (1992). https://doi.org/10.1007/BF01414760

30. Zhao, W., Jiang, Z.L., Saito, T., Lin, J., Yu, H., Takayama, K.: Performance of a detonation driven shock tunnel. Shock Waves **14**(1–2), 53–59 (2005). https://doi.org/10.1007/s00193-004-0238-1

31. Jiang, Z., Lin, J., Zhao, W.: Performance tests of JF-10 high-enthalpy shock tunnel with a FDC driver. Int. J. Hypersonics **2**(1), 29–36 (2012). https://doi.org/10.1260/1759-3107.2.1.29

32. Grabau, M., Smithson, H.K., Little, W.J.: A data reduction program for hotshot tunnels based on the Fay–Riddell heat transfer rate using nitrogen at stagnation temperatures from 1500 to 5000 K. Technical report AEDC- TDR-64-50 (1964)

33. Simeonides, G.: Hypersonic shock wave boundary layer interactions over compression corners. PhD thesis, von Karman Institute for Fluid Dynamics, University of Bristol (1992). https://doi.org/10.12681/eadd/28688

34. Hirschfelder, J.O., Buehler, R.J., McGee, H.A., Sutton, J.R.: Generalized equation of state for gases and liquids. Ind. Eng. Chem. **50**, 375–385 (1958)

35. Culotta, S., Enkenhus, K.R.: Analytical expressions for the thermodynamic properties of dense nitrogen. Technical note VKI-TN-50 (1968)

36. Jiang, Z., Takayama, K., Chen, Y.: Dispersion conditions for non-oscillatory shock capturing schemes and its applications. Comput. Fluid Dyn. J. **4**, 137–150 (1995)

37. Jiang, Z.: On dispersion-controlled principles for non-oscillatory shock-capturing schemes. Acta Mech. Sin. **20**, 1–15 (2004). https://doi.org/10.1007/BF02484239

38. Jiang, Z., Han, G., Wang, C., Zhang, F.: Self-organized generation of transverse waves in diverging cylindrical detonations. Combust. Flame **156**, 1653–1661 (2009). https://doi.org/10.1016/j.combustflame.2009.02.012

39. Jiang, Z., Takayama, K.: An investigation into the validation of numerical solutions of complex flow fields. J. Comput. Phys. **151**, 479–497 (1999). https://doi.org/10.1006/jcph.1999.6186

40. Spalart, P.R., Allmaras, S.R.: A one-equation turbulence model for aerodynamic flows. 30th Aerospace Sciences Meeting and Exhibit, Reno, NV, U.S.A., AIAA Paper 92-0439 (1992). https://doi.org/10.2514/6.1992-439

41. Luo, C.T., Wang, Y.P., Wang, C., Jiang, Z.L.: Wave system fitting: a new method for force measurements in shock tunnels with long test duration. Mech. Syst. Signal Process. **62–63**, 296–304 (2015). https://doi.org/10.1016/j.ymssp.2015.02.024

42. Penland, J.A.: Aerodynamic force characteristics of a series of lifting cone and cone-cylinder configurations at M = 6.83 and angles of attack up to 130°. NASA TN D-840 (1961)

43. Ladson, C., Blackstock, T.: Air-helium simulation of the aerodynamic force coefficients of cones at hypersonic speeds. NASA TN D-1473 (1962)

44. Zhang, H.: Hypersonic Aerodynamic Test. National Defense Industry Press, Beijing (2004)

45. Cheng, H.K.: Hypersonic shock-layer theory of a yawed cone and other three-dimensional pointed bodies. WADC TN 59–335 (1959)

46. Cheng, H.K.: Hypersonic flows past a yawed circular cone and other pointed bodies. J. Fluid Mech. **12**(2), 169–191 (1962). https://doi.org/10.1017/s0022112062000142

47. Ma, J., Tang, Z., Zhang, X.: Free flight method in hypersonic impulse type tunnels for static and dynamic stability study. Acta Aerodyn. Sin. **4**, 82–90 (1983). **(in Chinese)**

48. Fluid Dynamics Panel Working Group 15. Quality assessment for wind tunnel testing. AGARD-AR-304 (1994)

49. AIAA Standard: Assessment of experimental uncertainty with application to wind tunnel testing (AIAA S-071A-1999). American Institute of Aeronautics and Astronautics, VA, USA (1999). https://doi.org/10.2514/4.476648.001

50. AIAA Guide: Assessing experimental uncertainty-supplement to AIAA S-071A-1999 (AIAA G-045-2003). American Institute of Aeronautics and Astronautics, VA, USA (2003). https://doi.org/10.2514/4.476648.001

51. Anderson, J.D.: Hypersonic and High-Temperature Gas Dynamics, 2nd edn. American Institute of Aeronautics and Astronautics, Reston (2006). https://doi.org/10.2514/4.861956

52. MacWherter, M., Noack, R.W., Oberkampf, W.L.: Evaluation of boundary-layer and parabolized Navier–Stokes solutions for re-entry vehicles. J. Spacecr. Rockets **23**(1), 70–78 (1986). https://doi.org/10.2514/3.25085

53. Yang, Y., Wang, F., Guo, D.: Force measurement of the cone with 10° semivertex angle using a six-component balance system in the hypersonic impulse wind tunnel. Aerodyn. Exp. Meas. Control **2**(1), 60–64 (1988). **(in Chinese)**

54. Koppenwallner, G.: Fundamentals of hypersonics: aerodynamics and heat transfer. VKI Short Course notes Hypersonic Aerothermodynamics (1984)

55. Gray, J.D.: Summary report on aerodynamic characteristics of standard models hb-1 and hb-2. AEDC-TDR-64-137 (1964)

56. Hirschel, E.H.: Basics of Aerothermodynamics. Springer, Berlin (2005). https://doi.org/10.1007/b137734